Honorable Mention Poster Award

Dynamic Dosimetry and Edema Detection in Prostate Brachytherapy - a Complete System

A. Jain[1], A. Deguet[1], I. Iordachita[1], G. Chintalapani[1], J. Blevins[3], Y. Le[2], E. Armour[2], C. Burdette[3], D. Song[2], G. Fichtinger[4]
1 - Johns Hopkins University; 2 - Johns Hopkins School of medicine; 3 - Acoustic MedSystems Inc.; 4 - Queen's University

ABSTRACT

Purpose: Brachytherapy (radioactive seed insertion) has emerged as one of the most effective treatment options for patients with prostate cancer, with the added benefit of a convenient outpatient procedure. The main limitation in contemporary brachytherapy is faulty seed placement, predominantly due to the presence of intra-operative edema (tissue expansion). Though currently not available, the capability to intra-operatively monitor the seed distribution, can make a significant improvement in cancer control. We present such a system here.

Methods: Intra-operative measurement of edema in prostate brachytherapy requires localization of inserted radioactive seeds relative to the prostate. Seeds were reconstructed using a typical non-isocentric C-arm, and exported to a commercial brachytherapy delivery system. Technical obstacles for 3D reconstruction on a non-isocentric C-arm include pose-dependent C-arm calibration; distortion correction; pose estimation of C-arm images; seed reconstruction; and C-arm to TRUS registration.

Results: In precision-machined hard phantoms with 40-100 seeds and soft tissue phantoms with 45-87 seeds, we correctly reconstructed the seed implant shape with an average 3D precision of 0.35 mm and 0.24 mm, respectively. In a DoD Phase-1 clinical trial on 6 patients with 48-82 planned seeds, we achieved intra-operative monitoring of seed distribution and dosimetry, correcting for dose inhomogeneities by inserting an average of 4.17 (1-9) additional seeds. Additionally, in each patient, the system automatically detected intra-operative seed migration induced due to edema (mean 3.84 mm, STD 2.13 mm, Max 16.19 mm).

Conclusions: The proposed system is the first of a kind that makes intra-operative detection of edema (and subsequent re-optimization) possible on any typical non-isocentric C-arm, at negligible additional cost to the existing clinical installation. It achieves a significantly more homogeneous seed distribution, and has the potential to affect a paradigm shift in clinical practice. Large scale studies and commercialization are currently underway.

Keywords: Fluoroscopic guidance, Prostate brachytherapy, Low cost, Edema.

1. INTRODUCTION

With an annual incidence of over 200,000 new cases & 33,000 deaths in the US, prostate cancer continues to be the most common cancer in men,[1] and is expected to double its incidence rates by 2015. Currently one in every six men get diagnosed with it at some point in their life. For several decades, the definitive treatment for low risk prostate cancer was radical prostatectomy or external beam radiation therapy (EBRT). However, developments in prostate brachytherapy have seen it emerge as a primary treatment option, with recent studies showing an overall 15-year survival rate of 74% (88%, 80% & 53% in low, intermediate & high-risk patients). Improved patient selection and implant quality has resulted in multiple brachytherapy reports demonstrating survival rates equivalent to the best published radical prostatectomy and EBRT outcomes.[2] This has lead to a large increase in the number of brachytherapy procedures, with 30%-40% of all prostate cancer patients receiving brachytherapy as part of their treatment,[3] while utilization rates for prostatectomy and external-beam radiotherapy have fallen by over 10%. It is currently estimated that at over 50,000 brachytherapy procedures are performed annually.

Brachytherapy is a convenient one-time outpatient procedure, without the surgical trauma of prostatectomy or the grinding routine of EBRT. In this treatment a number of small ($\sim$ 1x5 mm) radioactive capsules are implanted into the prostate to kill the cancer by emitting radiation. It was first performed in 1911 with limited

Medical Imaging 2008: Visualization, Image-guided Procedures, and Modeling, edited by Michael I. Miga, Kevin Robert Cleary, Proc. of SPIE Vol. 6918, 69181Y, (2008)
1605-7422/08/$18 · doi: 10.1117/12.772352

success. In the 1960's, the use of Au-198 & I-125 isotopes triggered modern day permanent seed implantation. Many new techniques were introduced, but their limitations prevented widespread adoption. Nevertheless, it was found that disease control was better in early-stage patients who received high-quality implants (60% versus 20% local control).[3] The advent of transrectal ultrasound (TRUS)-guided procedures in the 1980's, along with computerized planning, lead to an increase in seed placement accuracy and a superior distribution of the seeds throughout the prostate. Early results showed that patients treated between 1988-90, performed better than those treated by the same physicians between 1986-87, the only difference being the quality of the implant. This further supported the hypothesis that higher-quality implants resulted in better outcomes. As the procedure has become more and more popular, many technical improvements have been added (eg. inverse planning and post-op CT) to improve the implant quality.

With virtually all studies agreeing that a high quality implant is the key to successful outcomes, the next paradigm shift is expected to be the capability to intra-operatively monitor the inserted seeds. The biggest bottleneck toward this, is seed migration induced by edema. This causes insufficient dose to the cancer and/or excess radiation to the rectum, urethra, and bladder. Edema is a natural response of the body, wherein the tissue expands due to the needle-insertions and radiation. Studies have shown that edema could increase the prostate volume by up to 100%, decreasing exponentially with time (mean half-life of 9.3 days), and potentially underdosing some patients by as much as 32%.[4] A small fraction of brachytherapy patients suffer from adverse side-effects like secondary malignancies in the rectum & bladder(7.6%[5]). Minor side-effects include temporary urinary symptoms (50-80%[6]), rectal bleeding (2-5%[3]) and sexual impotency (20%[3]). All these side-effects stem from imperfect execution of the intended plan, mostly due to edema. Thus, with the emphasis shifting to quality of life after treatment, intra-operative monitoring of seed distibution has become the holy grail.

In order to avoid over/under-dosing, the seed locations need to be determined intra-operatively, which is difficult, owing to significant seed migration due to edema. Contemporary research has tried to monitor the seeds from TRUS images by linking seeds with spacers,[7] using X-rays to initialize segmentation,[8] using vibro-acoustography,[9] transurethral ultrasound[10] as a new imaging modality, or segmenting them directly in TRUS images,[11] sometimes by using specially manufactured corrugated seeds that are better visible than conventional ones.[12] But even when meticulously hand-segmented, up to 25% of the seeds remain hidden in TRUS.[13] The seeds have excellent visibility under X-rays, with C-arms being ubiquitous (60% availability) in brachytherapy for gross visual assessment.[14] In spite of significant efforts that have been made towards computational fluoroscopic guidance in general surgery,[15] C-arms cannot yet be used for intra-operative brachytherapy guidance due to a plethora of technical limitations. While several groups have published protocols and clinical outcomes favorably supporting C-arm fluoroscopy for intra-operative dosimetric analysis,[16–18] this technique is yet to become a standard of care across hospitals. The most important current limitation towards a standard of care system, is the inability to use a non-isocentric C-arm, the type most commonly found in hospitals.

To achieve intra-operative monitoring in prostate brachytherapy, we report a new system that reconstructs 3D seed locations (visible in X-ray) and spatially registers them to the prostate (visible in TRUS). We discuss briefly the variety of technical issues in Section 2, following up with results from phantom experiments & a Phase-I clinical trials in Section 3. Our primary contribution to the state of the art is our ability to use any typical non-isocentric uncalibrated C-arm present in most hospitals. We believe that the availability of this technology, followed up with large scale clinical studies and commercialization (ongoing), promises to lead to a paradigm shift in the standard of care for image-guided prostate brachytherapy.

2. METHODS AND MATERIALS

The system is designed to easily integrate easily with commercial brachytherapy installations. We employ a regular clinical brachytherapy setup, without alteration, including a treatment planning workstation & stabilizer/stepper (Interplant®, CMS, St Louis), TRUS (B&K Medical Pro Focus) and a C-arm (GE OEC 9600/9800). The C-arm is interfaced with a laptop through an NTSC video line and frame grabber, making the image capture independent of the C-arm model.

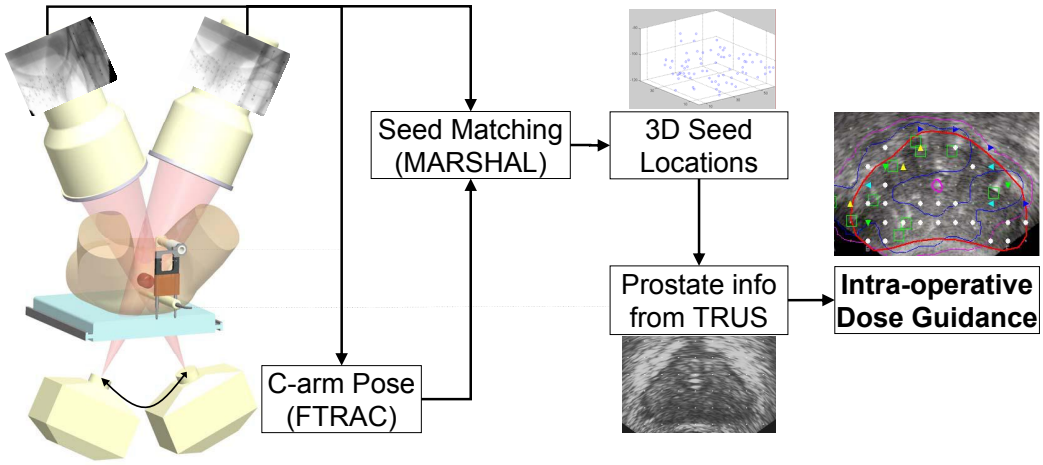

Figure 1. Overview of the proposed solution. The FTRAC fiducial tracks C-arms, and also registers TRUS to C-arm images, making quantitative brachytherapy possible.

Workflow: The clinical workflow (Fig. 1) is identical to the standard procedure until the clinician decides to run a reconstruction and optimization. A set of C-arm images are collected with *a separation as wide as clinically possible* (usually 10^o around AP-axis) and synchronously transferred to the laptop. After processing the images, the seeds are reconstructed and their 3D locations exported to the Interplant® system. The physician uses standard Interplant® tools to analyze, optimize and modify the remainder of the plan. The procedure concludes when the exit dosimetry shows no cold spots (under-radiated locations).

Numerous technical obstacles have to be overcome to realize C-arm based intra-operative dosimetry: (a) pose estimation of C-arm images; (b) C-arm calibration; (c) image distortion correction; (d) seed segmentation; (e) seed matching & reconstruction; (f) registration of C-arm to TRUS; (g) dosimetry analysis; and finally (h) implant optimization. We have developed a system that overcomes these limitations in providing quantitative intra-operative dosimetry. In what follows, we will describe briefly each component of the system, skipping the detailed mathematical framework.

Pose Estimation: The most critical component of a clinically usable solution for 3D fluoroscopic guidance is C-arm pose estimation. C-arms available in most hospitals do not have encoded rotational joints, making the amount of C-arm motion unavailable. C-arm tracking using auxiliary trackers is expensive, inaccurate in the presence of metal (EM tracking) or intrudes in the operating room (optical tracking). There has been some prior work on fiducial based tracking, wherein a fiducial is introduced in the X-ray FOV and its projection in the image encodes the 6 DOF pose of the C-arm. The most significant problem in contemporary designs is that though sufficiently accurate, they are too bulky to be easily used in a clinical setting. To improve clinical usability, the size of the fiducial can be decreased, usually at a significant expense of the accuracy.

We proposed a new fluoroscope tracking fiducial design, FTRAC, that uses an ellipse.[19] The fiducial is illustrated in Figure 2, 5. The ellipse makes pose recovery accurate by (a) always projecting as an ellipse; (b) allowing an accurate segmentation; and (c) providing closed form Jacobian formulations for fast optimization. The FTRAC design has salient features, including small dimensions (3x3x5cm), no special proximity requirements to the anatomy, and is relatively inexpensive. In particular, the small size makes it easier to be always in the FOV & to be robust to image distortion. Extensive phantom experiments indicated a mean tracking accuracy on distorted C-arms of 0.56 mm in translation and 0.19^o in rotation, an accuracy comparable to expensive external trackers.

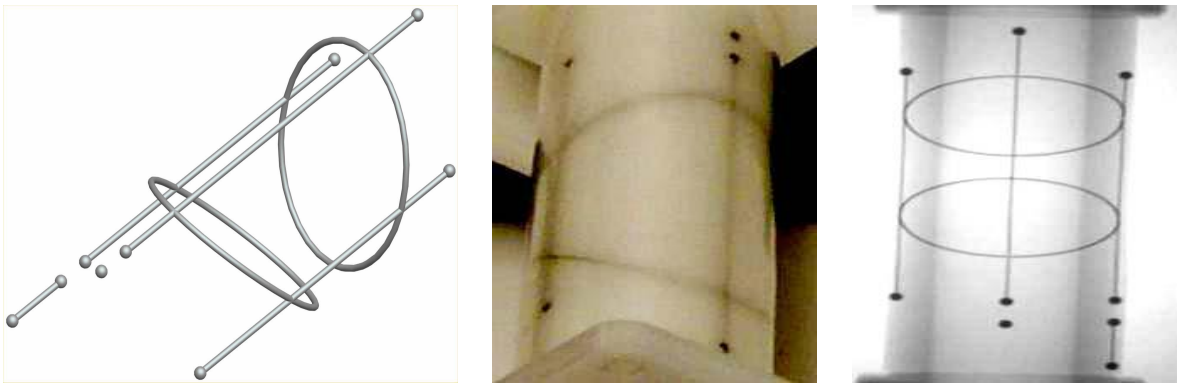

(a) (b) (c)

Figure 2. Images of the FTRAC fiducial (a) wire model; (b) photograph; (c) X-ray image

C-arm Source Calibration and Image Distortion: Since both C-arm calibration and distortion are pose-dependent, contemporary fluoroscopy guidance systems calibrate/ distortion-correct at each imaging pose. This is done using a cumbersome calibration-fixture, which is a significant liability. Our approach is a complete departure. Using a mathematical & experimental framework, we demonstrated that calibration is not critical for prostate seed reconstruction; *i.e.* just an approximate pre-operative calibration suffices. The central intuition is that object reconstruction using a mis-calibrated C-arm changes only the absolute positions of the objects, but not their relative ones (Fig. 3). Additionally, statistical analysis of the distortion on a GE OEC 9600, inside a 15^o limited workspace revealed that just a single pre-operative correction at the AP-axis can reduce the average distortion in the image from 3.31 mm to 0.51 mm. These errors are expected to be similar for most modern C-arms, with a more involved discussion available in.[20] This residual amount of distortion in the X-ray image is acceptable for accurate 3D reconstruction, especially when used with image based C-arm tracking.

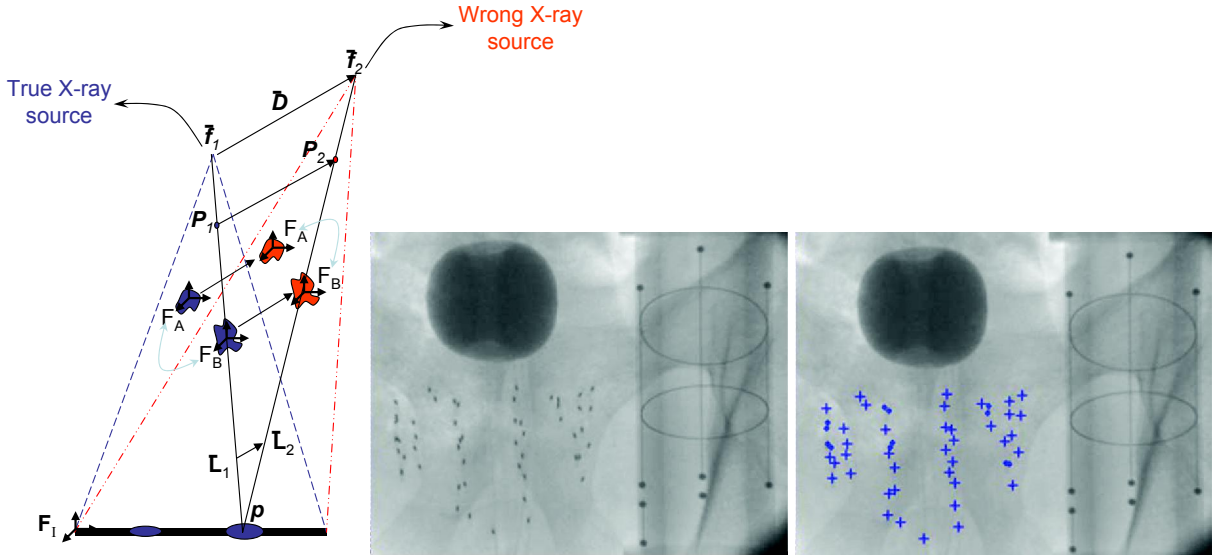

(a) (b)

Figure 3. (a) Mis-calibration conserves relative reconstruction between objects A and B (eg. seeds). (b) X-ray image before segmentation (left). There is also the FTRAC in the image. The image after segmentation (right); the blue '+' symbol represent individual seeds and the blue '.' indicates a seed that is a part of a multiple seed cluster.

Seed Segmentation: Seed segmentation in C-arm video images is usually hindered by poor image resolution. We developed an automated seed segmentation algorithm that employs the morphological top-hat transform to perform the basic seed segmentation, followed by thresholding, region labeling, and finally a statistical classification into two classes - single seeds and clusters containing overlapping seeds. Using some simple ellipse partitioning techniques, these clustered seeds are finally broken down into single seeds. The algorithm was tested on clinical images and found to be sufficiently accurate. Out of total 763 seeds from 10 patient images of Palladium implants, 758 seeds were correctly identified; only 2 seeds clusters were not correctly resolved and 2 false positives were added. The segmentation is verified on the screen to allow for a manual bypass by the surgeon.

Seed Correspondence & Reconstruction: The 3D coordinates of the implanted seeds can now be triangulated by resolving the correspondence of seeds in the multiple X-ray images. As explained in[21] we formalized the seed correspondence as a combinatorial optimization problem. As seen in Figure 4, a network is created where any flow represents a matching, the desired solution being the flow with minimum cost, computed using the cycle-canceling algorithm. Our formulation has many preferred features: (a) exact solutions; (b) claims on the problem complexity; and (c) optimality considerations. We showed that a polynomial-time perfect solution is not achievable and proposed a practical solution (MARSHAL) that runs practically in $O(N^3)$ using any number of images, where N is the number of inserted seeds. In comparison, previous solutions have predominantly been heuristic explorations of the large search space. In addition, the framework robustly resolves all the seeds that are hidden in the images (as many as 7% can be hidden due to the high seed density). A simple extension to the network at strategic nodes, allowing a flow of 2 units instead of 1, enables MARSHAL to also automatically recover hidden seeds. MARSHAL typically reconstructs 99.8% of the seeds and runs in under 5s in MATLAB, exhibiting a significantly higher than the required minimum-detection-rate of 95% that has been suggested.[22]

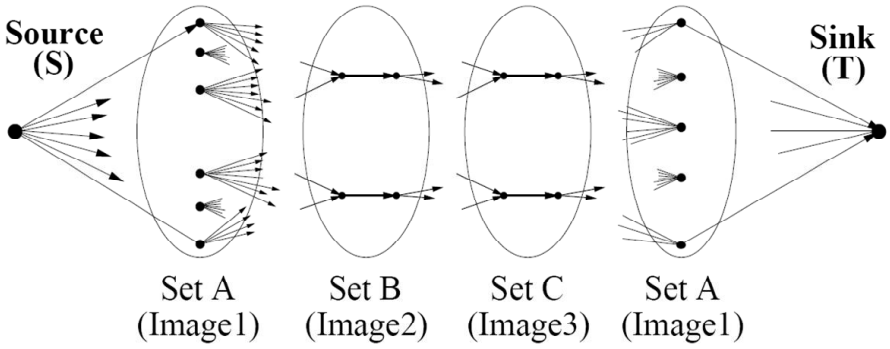

Figure 4. The network flow formulation used to solve the hidden-seed correspondence problem.

Registration of C-arm to TRUS: The 3D seed coordinates are reconstructed with respect to the FTRAC and need to be registered to the prostate boundaries visible in the TRUS images. This is a difficult problem, owing to the lack of physical access to the patient-anatomy and the inherently complementary natures of the two modalities. X-rays predominantly images hard tissue, while Ultrasound looks at soft tissue boundaries. In a quick survey of X-ray to TRUS registration, various groups have attempted to use catheters, gold marker seeds, needles or the inserted radioactive seeds as markers. Unfortunately, implanted markers in Ultrasound are very hard to differentiate from various other objects like inserted seeds & needle tracts. Moreover, they are also susceptible to intra-operative tissue expansion, making the registration unreliable. Alternately, radio-opaque beads were attached to the probe and have been used for registration, requiring a permanent alteration to the probe, which for many practitioners is not desirable. Altogether, a comprehensive and clinically reliable solution for spatial registration of fluoroscopy and TRUS images is currently not known.

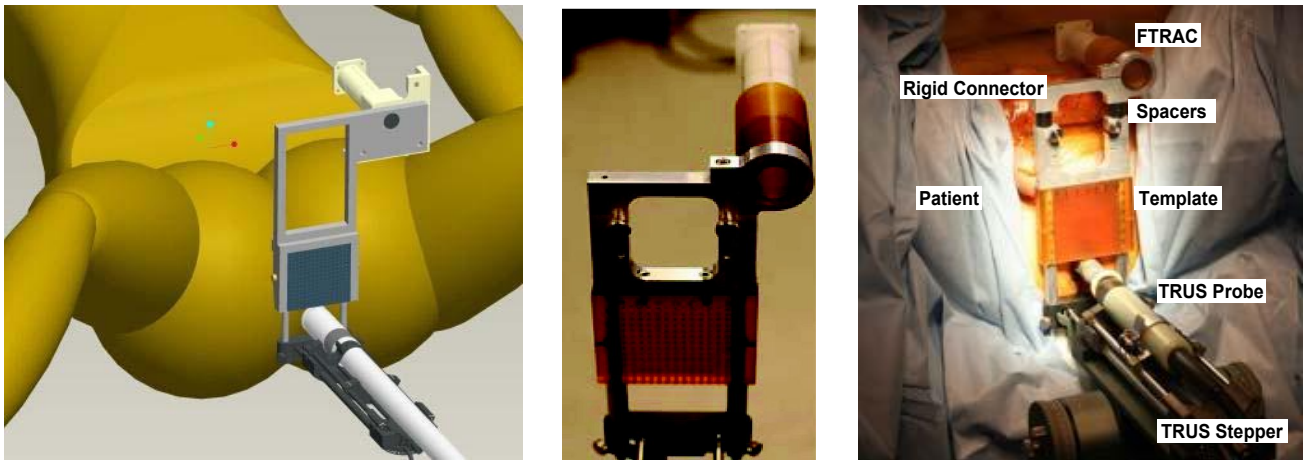

(a) (b) (c)

Figure 5. The FTRAC fiducial & the needle insertion template can be pre-calibrated using a rigid mount.(a) A CAD model of the FTRAC fiducial mounted on the seed-insertion needle template using a rigid connector. (b) An actual photograph of the FTRAC mounted on the template.(c) A zoomed annotated photograph of the clinical setup.

In commercial brachytherapy systems the needle insertion template is already pre-registered to TRUS probe as per the FDA approved clinical protocol. Hence, we propose to mount the FTRAC fiducial on top of this template in a known rigid position, using a precision-machined mechanical connector. The arrangement is illustrated in Figure 5. Thus a simple application of the various known frame transformations, registers the 3D seeds (FTRAC) to the prostate (TRUS).

System Implementation: We have integrated the previously discussed functions into a complete MATLAB program with a graphical user interface. Screen-captures from the program are shown in Figure 6. The package runs on an ordinary laptop that sends reconstructed seed positions to Interplant® system. In order to not require a new FDA approval, we maintain the integrity of the FDA-approved Interplant® system by not modifying the commercial software. We instead use a text file to export the 3D seed locations.

Dosimetry Analysis and Implant Optimization: The seed locations (in template coordinates) are exported to the Interplant® system. A software patch added to the Interplant® removes the already implanted seeds from the original plan, thereby producing a *"residual implant plan"*. The total dose is calculated by combining the current seed locations and those in the residual implant plan. The physician at this stage, modifies the residual plan to avoid any potential 'hot spots' (prostate tissue receiving significantly more than prescribed radiation dose), and most importantly, fills in any observed cold spots (under-dosed prostate tissue receiving less than prescribed radiation). This process can be repeated any number of times during the surgery, achieving a more homogenous seed distribution.

Clinical Workflow: The procedure flows in two main branches as shown in Figure 6 (b). In addition to the FDA approved TRUS-template calibration, the pre-operative phase now also includes the C-arm calibration. Intra-operatively, the procedure proceeds without any alterations. At any point, the physician can decide to incorporate the current 3D seed locations, in which an X-ray reconstruction is carried out. The TRUS probe is retracted to prevent the transducer from blocking the C-arm's field of view. With moving the C-arm over the target area, 3-4 X-ray images are collected. Each image provides a view of the prostate (with the implanted seeds) and the FTRAC fiducial. These images are automatically captured by the computer using a framegrabber. The intra-operative workflow continues with extensive image analysis, as described so far. Each C-arm image is

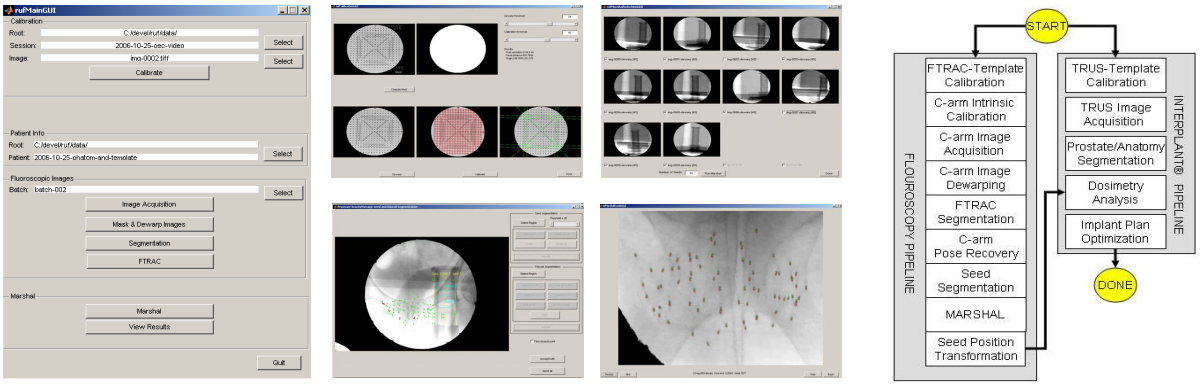

(a) (b)

Figure 6. (a) GUI screen captures of the main program, offline calibration, seed & fiducial segmentation, seed matching and validation of the reconstruction by back-projection. (b) Workflow for intra-operative dose optimization.

automaatically corrected for distortion. Next, the segmentation algorithm segments the motifs of the FTRAC fiducial and recovers the relative poses of the C-arm images, followed by the segmentation of all visible seeds in the images. MARSHAL then matches all the segmented seeds and reconstructs their 3D locations, while also recovering the seeds hidden in one or more images. Finally, we apply the predetermined coordinate transformation to the seed cloud to obtain the position of the seeds in template coordinates and send them to the Interplant®, where the dose coverage relative to the relevant anatomy is analyzed and the remainder of the implant plan optimized. At this point, the clinical workflow reeverts back to the default standard of care protocol.

3. PHANTOM EXPERIMENTS AND RESULTS

We have extensively tested the system and its components in various phantoms and in a Phase-1 clinical trial. To do so, we introduce the terms **absolute** and **relative** reconstruction errors. Using X-ray images, the seeds are reconstructed with respect to the FTRAC frame. In experiments where the ground truth location of the seeds with respect to the FTRAC is known, the comparative analysis of the seed locations is called **absolute** accuracy. Sometimes (eg. in patients), the true seed locations with respect to the FTRAC are not available and the reconstruction can only be compared to the seeds extracted from post-operative data (using a rigid point-cloud to point-cloud transform), in which case the evaluation is called **relative** accuracy.

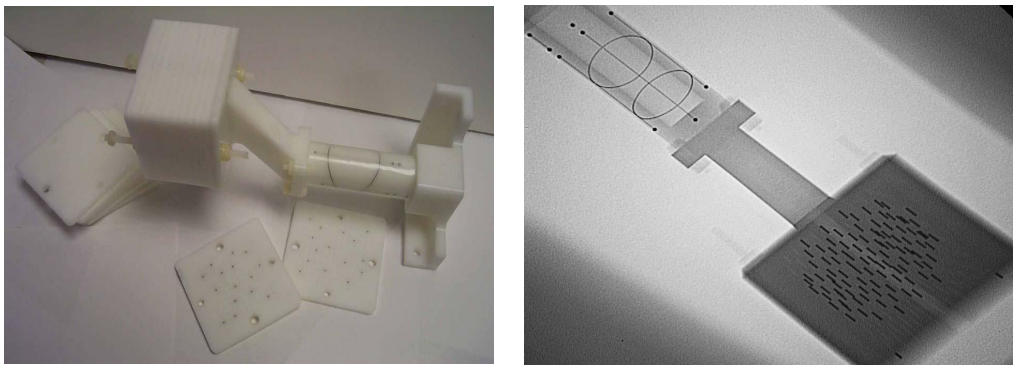

(a) (b)

Figure 7. (a) An image of the seed phantom attached to the FTRAC fiducial. The phantom can replicate any implant configuration, using the twelve 5 *mm* slabs each with over a hundred holes. (b) A typical X-ray image of the combination.

Solid Seed Phantom: An acetol (Delrin) phantom consisting of ten slabs (5mm each) was fabricated (Figure 7). This phantom provides a multitude of implants with sub-mm ground truth accuracy. The fiducial was *rigidly* attached to the phantom in a known way, establishing the accurate ground truth 3D location of each seed. Realistic prostate implants (1.56 seeds/cc, 40-100 seeds) were imaged within a 30^o cone around the AP-axis. The true correspondence was manually established by using the 3D locations, known from the precise fabrication. Averaged results indicate that we correctly match 98.5% & 99.8% of the seeds using 3 & 4 images (100 & 75 total trials) respectively. The mean 3D absolute reconstruction accuracy was 0.66 mm (STD 0.29 mm), while the relative accuracy was 0.35 mm. Furthermore, using 4 images yielded only one poorly mis-matched seed from the 75 datasets, suggesting the use of 4 images for better clinical guidance.

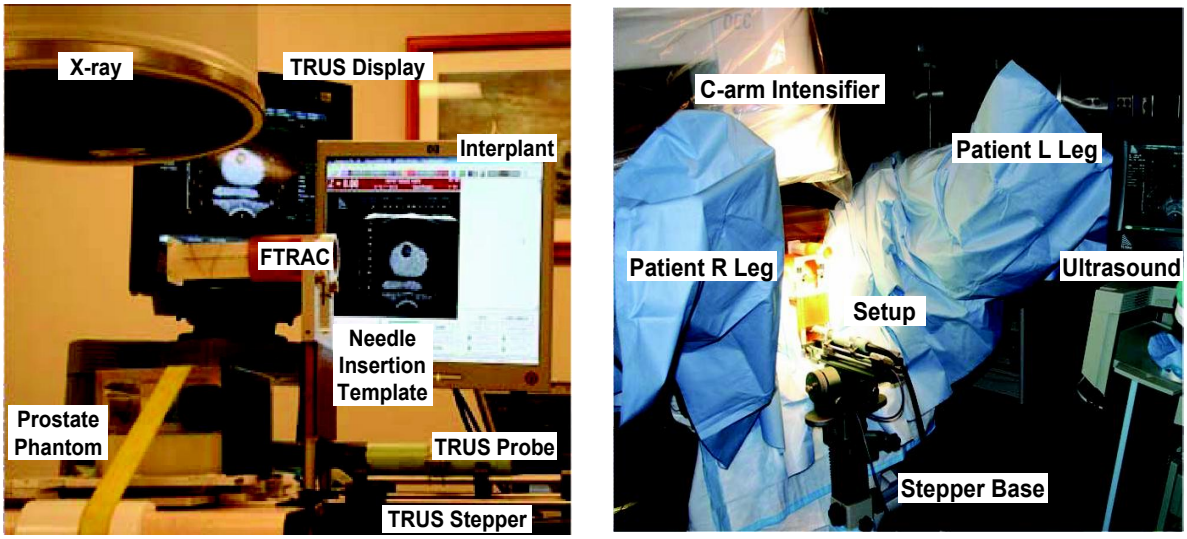

(a) (b)

Figure 8. An annotated image of the (a) experimental setup for the training phantom experiments; (b) overall set up of the full operating area during the Phase-I clincal trials.

Soft Training Phantoms: As annotated in Figure 8, we fully seeded three standard prostate brachytherapy phantoms with realistic implant plans (45, 49, 87 seeds). Seed locations reconstructed from fluoro using realistic (maximum available clinically) image separation (about 15^o) were compared to their corresponding ground truth locations segmented manually in CT (1mm slice thickness). Additionally, the 45 & 87-seed phantoms were rigidly attached to the FTRAC, providing the absolute ground truth (from CT). The 49-seed phantom was used to conduct a full scale practice-surgery, in which case the 3D reconstruction could be compared only to the seed cloud from post-op CT (without FTRAC), providing just relative accuracy.

The performance of the system on the soft tissue training phantoms is tabulated in Table 1. The absolute reconstruction errors for the 45, 87-seed phantoms were 1.64 mm & 0.95 mm (STD 0.17 mm), while the relative reconstruction errors for the 45, 49, 87-seed phantoms were 0.22 mm, 0.29 mm, 0.20 mm (STD 0.13 mm). A mean translation shift of 1.32 mm was observed in the 3D reconstructions, predominantly due to the limited C-arm workspace (solid-phantom experiments with 30^o motion have 0.65 mm accuracy). It was observed that the shift was mostly random & not in any particular direction. In fact, it was noticed that if different combinations of the X-ray images were used, it would result in different directions for the overall shift. This suggests that the shift is most probably due to the small amounts of error (sub-mm, sub-degree) in the pose estimation part of the system. Note that *our reconstruction accuracy is better than the CT resolution* (as evident from the solid seed phantom experiments). Moreover, the 3D error is larger in the Z-direction, which corresponds to the direction

Number of Seeds	Error Type	Error (mm) X	Y	Z	3D Error (mm)	Translation Offset (mm)
45	Absolute	0.38	0.94	1.27	1.64	1.50
87		0.41	0.40	0.71	0.95	1.13
	***A*verage**	*0.40*	*0.67*	*0.99*	*1.30*	*1.32*
45	Relative	0.08	0.14	0.12	0.22	-
49		0.09	0.11	0.10	0.29	-
87		0.12	0.18	0.12	0.20	-
	***A*verage**	*0.10*	*0.14*	*0.11*	*0.24*	-

Table 1. Tabulated performance of the system on soft tissue training phantoms. Note the difference between the absolute and relative reconstruction errors.

of the 1 mm axial slices of the CT. Nevertheless, the accuracy is sufficient for brachytherapy, especially since a small shift does not hamper the ability to detect the presence of any cold spots.

Patients: A total of 18 batches of reconstructions were carried out on 6 patients with $2-4$ batches/patient, as and when a need for dose evaluation was felt by the clinician. The number of seeds in each batch varied from $22-84$. Since the seeds migrate significantly by the time a post-operative CT is taken, there is no easy method for knowing the true 3D seed locations (ground truth) in real patients. Hence, for each reconstruction $4-6$ additional X-ray images were taken. The intra-operatively reconstructed 3D seed locations were projected on these additional images and compared to their corresponding segmented 2D locations (post-operatively). The results from a total of 99 such projections from 18 reconstructions are tabulated in Table 2.

Patient Number	Number of Seeds	Additional X-ray Images	Error in X-ray Image (mm) Mean	STD	Max	Min
1	22	6	2.32	0.21	2.75	1.92
	44	5	2.24	0.31	2.86	1.47
	65	5	1.19	0.29	1.95	0.52
	66	5	1.01	0.23	1.70	0.53
2	39	5	1.20	0.21	1.67	0.81
	84	4	2.16	0.60	4.18	0.35
3	33	5	1.19	0.27	1.88	0.63
	67	6	1.60	0.44	2.76	0.74
	70	4	1.47	0.64	3.22	0.38
4	35	5	1.21	0.21	1.64	0.75
	68	6	1.43	0.42	3.05	0.41
	77	5	1.81	0.29	2.59	1.15
5	24	6	2.30	0.45	3.09	1.46
	48	6	2.19	0.46	3.51	1.07
	53	7	2.17	0.41	3.40	1.51
6	33	6	1.90	0.32	2.67	1.34
	61	7	2.30	0.34	3.44	1.49
	66	6	1.40	0.29	2.14	0.76
Average	**56**	**5.5**	**1.57**	**0.34**	**2.50**	**0.83**

Table 2. 18 intra-operative 3D X-ray seed reconstructions with 22-84 seeds, projected back on additional 99 (unused) X-ray images. Note that the maximum error is never remarkably huge.

The results indicate a 2D mean error of 1.57 *mm* (STD 0.34 *mm*, max 2.50 *mm*, *min*0.83 *mm*). This indicates a sub-mm accuracy in 3D reconstruction, since the errors get magnified under a perspective transform when projected from 3D to a 2D image. Though the magnification factor varies for each image depending on the relative depth of the seeds with respect to the C-arm focal length, it ranges approximately from $1.5 - 2$. This indicates an average absolute 3D reconstruction accuracy of $0.8 - 1.0$ *mm*, which is similar to the results obtained from the phantom experiments. Further note that the average minimum error is 0.83 *mm*, indicating that there is a small consistent *shift/bias* in the reconstruction. This collaborates completely with the observations that were made earlier. In only one case (patient-2 84-seeds), we see a maximum error more than 4 mm. However, in this cases we also observe that the overall deviation is higher too, indicating that these datasets might have a larger 3D shift/bias. In any case, we do not see the maximum error go many deviations away from the mean error. A 2.5 mm error in 3D is expected to project as a 5 *mm* error at least in some of the X-ray images, which we have not observed. This indicates that we had successful intra-operative reconstructions in the Phase-I patient trials.

Registration Accuracy: To measure the accuracy of the fiducial-to-template registration, three batches of five straight needles each were inserted randomly at known depths (Z-axis) into known template holes (X, Y-axis). Their reconstructed tip locations with respect to the FTRAC coordinate-frame were transformed to the template coordinate-frame using our rigid registration transform, which were then compared to their true measured locations in template coordinates. The limited-angle image-capture protocol was kept similar to that used in the operating room. Both absolute and relative results are tabulated in Table 3. The average absolute error (reconstruction together with registration) was 1.03 mm (STD 0.18 mm), while the average relative error was 0.36 *mm* (STD 0.21 mm), with an average translation shift of 0.97 mm. Note that the performance of the system in these experiments is similar to the performance of the system in the other experiments presented so far, strengthening the validity of our conclusions.

Trial Number	**Error Type**	**Error (mm)**			**3D Error (mm)**	**Translation Offset (mm)**
		X	**Y**	**Z**		
1	Absolute	0.32	0.70	0.84	*1.16*	1.15
2		0.66	0.29	1.02	*1.27*	1.22
3		0.12	0.28	0.54	*0.65*	0.55
1	Relative	0.11	0.17	0.05	*0.22*	-
2		0.10	0.27	0.35	*0.49*	-
3		0.10	0.27	0.19	*0.36*	-

Table 3. 3 sets of 5 needles were inserted into the template at known depths and reconstructed. This comparison gives us the cumulative 3D error from X-ray reconstruction with respect to FTRAC and FTRAC-template registration, *i.e.* 3D reconstruction error with respect to the template.

System Accuracy: To measure the full system error, 5 needles (tips) were inserted into a prostate brachytherapy training phantom, reconstructed in 3D and exported to the Interplant® software. The needle tips were also segmented manually using TRUS images. The sagittal images were used for measuring the depth (Z-axis) of the needles and the transverse images were used to measure the planar positions (X,Y-axis), providing ground truth from Ultrasound. The mean absolute error for the 5 needle tips was 4 *mm* (STD 0.53 *mm*), with a translation shift of 3.94 mm. In comparison, the relative accuracy for the complete system was 0.83 *mm* (STD 0.18 mm).

The shift can mainly be attributed to (i) an error in the Template-TRUS pre-calibration done as part of current clinical practice, resulting in a shift ($\sim$ 3 mm); and (ii) a random bias in the 3D reconstruction due to limited image separation ($\sim$ 1 mm). Nevertheless, we removed this shift in the clinical cases by applying a translation-offset to the reconstructed X-ray seed coordinates. Owing to the small size of the prostate, the

rotation offset was always found to be minimal and could be ignored. The resultant translation offset was intra-operatively estimated by comparing the centroid of the reconstructed seeds with that of the planned seed locations, and by aligning the two together. Note that the centroid is a first-order statistic and robust to any spatially symmetric noise/displacement model. Though a heuristic, it provided excellent qualitative results according to the surgeon, who read the visual cues at the reconstructed seed locations in TRUS images. Based on the experiments so far and the surgeon's feedback, the overall accuracy of the system is expected to be $1-2\ mm$ during clinical use.

Phase-I Clinical Trial: We have treated a cohort of 6 patients, as part of a DoD Phase-I clinical trial to test the efficacy and safety of the system (the Phase-II trial is currently open for enrollment). Annotated photographs of the clinical setup are shown in Figure 5 (c) & 8 (b). Intra-operative dosimetry was performed (i) halfway during the surgery; (ii) at the end of the surgery; and (iii) after all the additional seeds were inserted. The current protocol adds about 15 minutes for each reconstruction, including the capture of 5 extra X-ray images for research validation, image processing, 3D seed reconstruction, and dosimetry optimization. In regular everyday clinical practice, we anticipate the need for only a single exit-dosimetry reconstruction, increasing the operating time only by about 10 minutes. *In all the patients the final dosimetry detected cold spots* (Figure 9). The clinician grew quickly to trust the system in detecting cold spots, and instead minimized potential hot spots during the surgery. The medical team found the intra-operative visualization of under-dosed regions valuable, inserting an additional 4.17 seeds on an average to make the 100% prescribed iso-dose contour cover the prostate. All patients were released from the operating room with satisfactory outcomes.

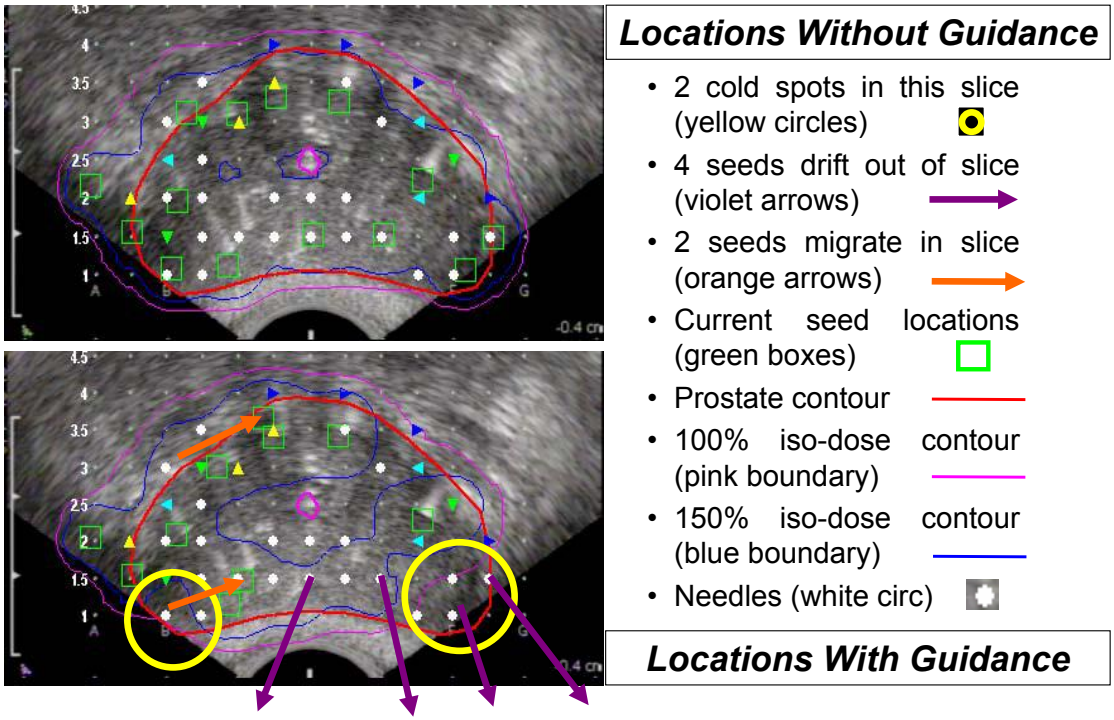

Figure 9. The system is able to detect cold spots. The seed locations (and corresponding 100/150% iso-dose contours) as **assumed** by the planning system (top) and as **computed** by the proposed system (bottom), discovering 2 cold spots in this slice. 4 seeds have drifted out of the slice, while 2 have migrated significantly within.

The *intra-operative detection and visualization of* ***edema*** *was also made possible* by the proposed system, as shown in Figure 10. Edema is the swelling of the prostate tissue due to the repeated stress from the punctures

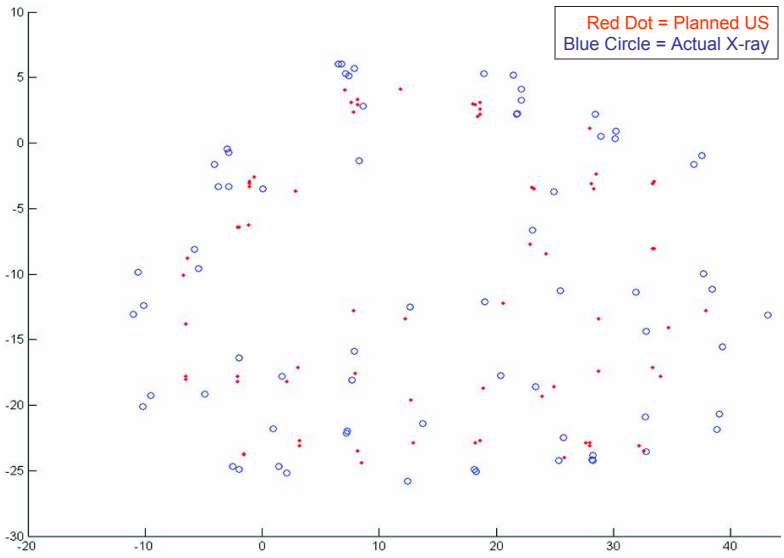

Figure 10. The system can visualize intra-operative edema, as seen for patient 3 (mean 4.6 mm, STD 2.4 mm, max 12.3 mm). The 'planned' (red) versus the 'reconstructed' (blue) seed positions as seen in the template view. A trend of outward dispersion from their initial locations is observed.

created by needle insertions and the high radioactivity from the dropped seeds. It is the single-most important source of bottleneck towards accurate dose delivery, arguably leaving behind cold spots. The system is unique, in that it is the first of a kind that can intra-operatively quantify the edema related seed migration. The system computed significant intra-operative edema in all the patients, with an average tissue expansion of 3.84 *mm* (STD 2.13 *mm*). *The seeds (and hence the prostate) showed a clear tendency for outward migration from their drop positions (with maximums up to 16 mm).* In all the patients, towards the end of the surgery, it was found that the apex of the prostate (surgeon-end) was under-dosed.

Comparison Type	**Error (mm)**			**Norm (mm)**		
	X	**Y**	**Z**	**Mean**	**STD**	**Max**
Pre-op TRUS to Day-0 Post-op CT (6 patients)	*1.93*	*2.30*	*2.28*	**4.39**	*2.60*	**14.25**
Pre-op TRUS to Day-30 Post-op CT (6 patients)	*2.07*	*2.19*	*2.55*	**4.56**	*2.78*	**17.47**
Day-0 Post-op CT to Day-30 Post-op CT (6 patients)	*1.62*	*2.00*	*1.93*	**3.78**	*2.72*	**17.31**

Table 4. The pre-operative planned 3D seed coordinates (TRUS) were compared to their corresponding post-operative locations computed from CT volumes. Significant seed migration due to edema can be observed.

A further comparison of the 3D final implant reconstructed using the X-ray images to Day-0 CT (2 mm slices) indicated an increased average post-operative edema of 4.39 *mm* (STD 2.60 *mm*), indicating a further post-operative seed migration in a few hours after the patient leaves the operating room. However, post-operative seed migration is an inherent limitation of brachytherapy, the best solution being a calculated intra-operative over-dosing of the patient. This makes the detection of any intra-operative edema even more critical. Brachytherapists have been traditionally accommodating for it by over-dosing the patient. Though effective, it involves some skilled qualitative guesswork on behalf of the surgeon, potentially limiting cancer control in difficult cases. Note that, in such a scenario, a sub-mm accuracy in the placement of the seeds inside the prostate could have a lesser impact on long-term cancer control.

Patient Number	Comparison Type	Error (mm) X	Y	Z	Norm (mm) Mean	STD	Max	Additional Seeds Added
1	Intra-op X-ray to Pre-op TRUS	0.26	0.41	0.45	0.77	1.09	9.00	**1**
2		1.91	1.88	3.18	4.65	2.20	12.23	**2**
3		2.50	2.13	2.28	4.59	2.36	12.26	**3**
4		1.59	1.57	2.68	4.27	2.53	16.02	**9**
5		1.61	2.67	3.05	4.98	2.83	16.19	**5**
6		1.47	2.30	1.88	3.78	1.76	9.82	**5**
Average		*1.56*	*1.83*	*2.25*	**3.84**	*2.13*	**12.59**	**4.17**
1	Intra-op X-ray to Day-0 Post-op CT	1.88	2.71	3.32	5.42	2.46	11.14	-
2		2.65	3.48	2.87	6.16	2.96	14.32	-
3		1.33	1.39	1.30	2.67	2.13	14.72	-
4		1.63	2.76	3.23	5.45	2.60	14.50	-
5		1.47	1.49	2.70	3.77	2.53	13.79	-
6		1.74	1.22	1.44	3.00	2.70	14.45	-
Average		*1.78*	*2.37*	*2.47*	**4.41**	*2.56*	**13.82**	-
1	Intra-op X-ray to Day-30 Post-op CT	2.64	3.62	2.57	5.78	2.49	12.04	-
2		3.45	3.84	2.86	6.84	3.32	21.75	-
3		2.04	2.55	2.13	4.70	1.97	11.17	-
4		1.70	2.40	1.87	4.07	2.14	12.51	-
5		2.45	3.27	2.83	5.70	3.10	21.87	-
6		0.97	1.51	1.67	2.91	2.42	12.49	-
Average		*2.21*	*2.87*	*2.32*	**5.00**	*2.57*	**15.31**	-

Table 5. The intra-operatively computed seed coordinates were compared those obtained from planned locations in TRUS and post-operative segmentations from CT. Additional seeds were added for each patient to close any detected cold spots.

4. CONCLUSION, SHORTCOMINGS AND FUTURE WORK

A system for intra-operative brachytherapy seed monitoring has been presented. In precision-machined hard phantoms with 40-100 seeds, we correctly reconstructed 99.8% seeds with a mean 3D accuracy of 0.35 mm. In soft tissue phantoms with 45-87 seeds & clinically realistic 15^o C-arm motion, we correctly reconstructed 100% seeds with an accuracy of 0.24 mm. 18 intra-operative reconstructions from a phase-I clinical study also show a correct 3D reconstruction with under 1 mm error. This accuracy is more than sufficient for accurate intra-operative monitoring of the plan, since the system was able to measure the extent of intra-operative seed migration, showing that it could be as high as 16.19 mm (mean 3.84 mm). The proposed work was also successfully used in a Phase-I DoD clinical trial, showing usefulness and great potential.

The system (a) requires no significant hardware; (b) does not alter the current clinical workflow; (c) can be used with any C-arm; (d) integrates easily with any pre-existing brachytherapy installation; & (e) is economically feasible and scalable. There is some added radiation to the patient from the X-ray images, though insignificant when compared to that from the radioactive seeds. Though not critical, primary shortcomings include (a) 15 minute additional surgery time; & (b) a small translation bias. Research is currently underway to remove these limitations, and to conduct large scale clinical studies using clinical indicators. Commercialization is also currently in progress. Furthermore, the proposed system is the first of its kind that can intra-operatively detect seed migration using any non-isocentric C-arm, achieving a significantly more homogeneous distribution and avoiding radiation hot/cold-spots. All the above put together, promises to lead to a paradigm shift in the standard of care for image-guided prostate brachytherapy, considerably improving the patient quality of life.

5. ACKNOWLEDGMENTS

This work has been supported by DoD PC050170 - Prostate Cancer Research Program (2005) pre-doctoral Traineeship Award, NIH SBIR 1R43CA099374 01, NSF EEC-9731478.

REFERENCES

1. A. Jemal, R. Siegel, E. Ward, T. Murray, J. Xu, C. Smigal, and M. Thun, "Cancer statistics," *CA Cancer J Clin* **56**(2), pp. 106–30, 2006.
2. Sylvester et al, "15-year biochemical relapse free survival in clinical stage t1-t3 prostate cancer following combined external beam radiotherapy and brachytherapy; seattle experience," *IJRBOP* **67**(1), 2007.
3. P. Grimm and J. Sylvester, "Advances in brachytherapy," *Urology* **6**(4), pp. 37–48, 2004.
4. Yue et al, "The impact of edema on planning 125i and 103pd prostate implants," *Med Phys* **26**(5), pp. 763–7, 1999.
5. Liauw et al, "Second malignancies after prostate brachytherapy: Incidence of bladder and colorectal cancers in patients with 15 years of potential follow-up," *IJROBP* **66**(3), pp. 668–73, 2006.
6. Langley et al, "European collaborative group on prostate brachytherapy: Preliminary report in 1175 patients," *European Urology* **46**(5), pp. 565–70, 2004.
7. J. Xue, E. Gressen, and T. Jefferson, "Feasibility of trus-based prostate post-implant dosimetry," in *AAPM annual meeting*, p. Poster, July 2004.
8. Dumane et al, "Combined ultrasound-fluoroscopy approach to the intraoperative detection of seeds in prostate brachytherapy," in *ASTRO annual meeting, Poster*, Oct 3-7 2004.
9. F. Mitri, P. Trompette, and J. Chapelon, "Improving the use of vibro-acoustography for brachytherapy metal seed imaging: A feasibility study," *IEEE Trans on Medical Imaging* **23**, pp. 1–6, Jan 2004.
10. D. Holmes, B. Davis, C. Bruce, and R. Robb, "3d visualization, analysis, and treatment of the prostate using trans-urethral ultrasound," *Comput Med Imaging Graph* **27**(5), pp. 339–49, 2003.
11. D. French, J. Morris, M. Keyes, and S. E. Salcudean, "Real-time dosimetry for prostate brachytherapy using trus and fluoroscopy," in *MICCAI (2) 2004*, pp. 983–991, 2004.
12. A. Tornes and M. Eriksen, "A new brachytherapy seed design for improved ultrasound visualization," in *IEEE Symposium on Ultrasonics*, pp. 1278–83, Oct 2003.
13. B. Han, K. Wallner, G. Merrick, W. Butler, S. Sutlief, and J. Sylvester, "Prostate brachytherapy seed identification on post-implant trus images," *Med Phys* **30(5)**, pp. 898–900, 2003.
14. B. Prestidge, J. Prete, T. Buchholz, J. Friedland, R. Stock, P. Grimm, and W. Bice, "A survey of current clinical practice of permanent prostate brachytherapy in the united states," *Int J Radiat Oncol Biol Phys* **15;40(2)**, pp. 461–5, Jan 1998.
15. R. Hofstetter, M. Slomczykowski, M. Sati, and L. Nolte, "Fluoroscopy as an imaging means for computer-assisted surgical navigation," *Comput Aided Surg* **4(2)**, pp. 65–76, 1999.
16. Reed et al, "Intraoperative fluoroscopic dose assessment in prostate brachytherapy patients," *Int J Radiat Oncol Biol Phys* **63**, pp. 301–7, Sep 2005.
17. D. Todor, M. Zaider, G. Cohen, M. Worman, and M. Zelefsky, "Intraoperative dynamic dosimetry for prostate implants," *Phys Med Biol* **48(9)**, pp. 1153–71, May 7 2003.
18. French et al, "Computing intraoperative dosimetry for prostate brachytherapy using trus and fluoroscopy," *Acad. Rad.* **12**, pp. 1262–72, Oct 2005.
19. A. Jain, T. Mustufa, Y. Zhou, E. C. Burdette, G. Chirikjian, and G. Fichtinger, "A robust fluoroscope tracking (ftrac) fiducial," *Med Phys* **32**, pp. 3185–98, Oct 2005.
20. Jain et al, "C-arm calibration: is it really necessary?," in *SPIE Medical Imaging 2007, Presented at the Society of Photo-Optical Instrumentation Engineers (SPIE) Conference* **6509**, Mar. 2007.
21. R. Kon, A. Jain, and G. Fichtinger, "Hidden seed reconstruction from c-arm images in brachytherapy," in *IEEE ISBI*, pp. 526–29, Apr 2006.
22. Su et al, "Examination of dosimetry accuracy as a function of seed detection rate in permanent prostate brachytherapy," *Med Phy* **32**, pp. 3049–56, Sep 2005.